Time-resolved X-ray microtomographic measurement of water transport in wood-fibre reinforced composite material

2016 IOP Conf. Ser.: Mater. Sci. Eng. 139 012037

(http://iopscience.iop.org/1757-899X/139/1/012037)

IOP Conf. Series: Materials Science and Engineering **139** (2016) 012037 doi:10.1088/1757-899X/139/1/012037

Time-resolved X-ray microtomographic measurement of water transport in wood-fibre reinforced composite material

Arttu Miettinen[1], Tero Harjupatana[1], Markku Kataja[1], Stefania Fortino[2], Kirsi Immonen[2]

[1] University of Jyväskylä, Department of Physics, P.O. Box 35 (YFL) FI-40014 Jyväskylä, Finland
[2] VTT Technical Research Centre of Finland, P.O. Box 1000, FI-02044 VTT, Finland

E-mail: arttu.miettinen@phys.jyu.fi

Abstract. Natural fibre composites are prone to absorb moisture from the environment which may lead to dimensional changes, mold growth, degradation of mechanical properties or other adverse effects. In this work we develop a method for direct non-intrusive measurement of local moisture content inside a material sample. The method is based on X-ray microtomography, digital image correlation and image analysis. As a first application of the method we study axial transport of water in a cylindrical polylactic acid/birch pulp composite material sample with one end exposed to water. Based on the results, the method seems to give plausible estimates of water content profiles inside the cylindrical sample. The results may be used, *e.g.*, in developing and validating models of moisture transport in biocomposites.

1. Introduction

Natural fibre composites appear as a promising and environmentally friendlier alternative for, *e.g.*, engineering plastics and glass fibre reinforced composites [1]. A main challenge with many natural-fibre reinforced thermoplastic composites is their inherent tendency to absorb water. This may lead to fungal decay, mold growth, mechanical degradation and dimensional instability, and thereby to, *e.g.*, decreased service life [1, 2]. A key topic in development of improved natural fibre composites is thus understanding the influence of moisture on the properties of the material, in particular if the material is to be used in variable environmental conditions.

Measuring time-dependent three-dimensional moisture content field inside material is a non-trivial task, especially for heterogeneous materials that contain multiple phases. In this work we present a method for measuring one-dimensional time-dependent water content profile based on three-dimensional X-ray microtomographic images. The method is based on first using 3D digital image correlation for measuring the displacement field of the wetted and possibly swollen sample. The local water content is then found by measuring the change in the values of the effective X-ray attenuation coefficient for each material point (3D image voxel) between the dry state and the wetted and deformed state.

Previously, several authors have used various methods based on X-ray tomography to determine local moisture content in different kinds of materials like stone, clothing and wood [3–6]. In many of those works the effects of swelling deformation of the material has not been

considered, or is included by making a specific assumption on the deformation characteristics of the material. Other possible methods for measuring local water concentration, based on sensing local amount of hydrogen nuclei in the material, are neutron radiography [7, 8] and magnetic resonance imaging [9].

A method similar to the one introduced in this paper was recently published and used for measuring water content in an approximately 2 cm wide bentonite clay sample [10]. Application of the method to smaller and less-absorbing composite material samples poses several problems in sample preparation, imaging and image analysis. Here, we demonstrate its practical application on a cylindrical polylactic acid/birch pulp composite material sample of diameter 2 mm. The experimental set-up was designed to yield one-dimensional axial wetting. Finally, the feasibility of the method is assessed based on the results from this first trial experiment.

2. Method for analysing moisture content distribution using X-ray tomography

We start by considering a composite material sample at known low water content, called the 'dry state' of the sample, in what follows. An X-ray tomographic image of the dry sample, denoted by $\mu^0_{\text{eff}}(\vec{x})$, $\vec{x} \in C \subset \mathbb{R}^3$, represents a three-dimensional map of the effective X-ray attenuation coefficient indicating the original reference configuration of the sample. Subjecting the sample to a moist environment initiates absorption of water and deformation due to swelling. Assuming that the absorption process is slow enough so that the state of the sample can be assumed approximately stationary within the tomographic scanning time used, we can take another X-ray tomographic image of the partially wetted sample during the wetting process. This image, denoted by $\mu_{\text{eff}}(\vec{x})$ now represents the wetted and deformed configuration of the sample. The task is now to find the distribution of water content of the wet state and express it in the reference frame defined by the dry sample.

To this end, we first estimate the displacement field $\vec{u}(\vec{x}) = (u_1(\vec{x}), u_2(\vec{x}), u_3(\vec{x}))$ between the dry state and the wet/deformed state using the images μ^0_{eff} and μ_{eff} representing these two states. Assuming that the swelling strain is small enables using a simple block-matching algorithm to find the displacement field. The algorithm is based on comparing displaced subregions of the wet state image to non-displaced subregion of the dry state image and minimizing the squared difference with respect to displacement, *i.e.*

$$\vec{u}(\vec{x}) = \text{argmin}_{\vec{u}' \in S} \sum_{\vec{y} \in W} (\mu_{\text{eff}}(\vec{y} + \vec{u}') - \mu^0_{\text{eff}}(\vec{y}))^2, \tag{1}$$

where S is a neighbourhood of origin and W is a neighbourhood of $\vec{x}$. The set S determines the possible values of the displacement and the set W gives the size of the subregion where the two images are compared.

For given displacement field $\vec{u}(\vec{x})$, a back-projected image of the wet state image is defined by

$$\mu^P_{\text{eff}}(\vec{x}) = \mu_{\text{eff}}(\vec{x} + \vec{u}(\vec{x})). \tag{2}$$

The image $\mu^P_{\text{eff}}(\vec{x})$ thus contains the values of attenuation coefficient of wet state material points associated with the original dry state positions of the same material points.

In addition to local change of partial density[1] of water ρ_w, wetting generally induces deformation and can therefore lead to local change of composite material (solid phase) partial density ρ_c, too. As the presence of both water and solid material contribute to local X-ray attenuation, the change in the water content can not be deduced based on the measured change of the local value of the X-ray attenuation coefficient alone. The necessary additional information

[1] Partial density of component α of a mixture is defined as $\rho_\alpha = m_\alpha / V$, where m_α is the mass of component α contained in volume V of the mixture.

can, however, be obtained utilizing the displacement field $\vec{u}(\vec{x})$ and using conservation of mass of the composite material. The change of ρ_c between the dry state and the wet state is thereby found to be

$$\Delta\rho_c(\vec{x}) = -\rho_c^0(\vec{x})\frac{\delta(\vec{x})}{1+\delta(\vec{x})}, \tag{3}$$

where $\rho_c^0(\vec{x})$ is the density of the composite material in the dry state, and

$$\delta(\vec{x}) = \nabla \cdot \vec{u}. \tag{4}$$

The local value of attenuation coefficient of X-rays can be assumed to depend linearly on local densities ρ_c and ρ_w in the wet composite material [11]. We thus write

$$\mu_{\text{eff}} = \alpha_c\rho_c + \alpha_w\rho_w, \tag{5}$$

where α_c and α_w are X-ray mass attenuation coefficients of the composite material and water, respectively (for the composite material, α_c is the mass averaged attenuation coefficient of its component materials). The coefficients α_c and α_w are unknown a priori and must be found by calibration measurements. The difference of the effective X-ray attenuation coefficient between the back-projected wet state and the dry state is given in the dry state reference frame by

$$\begin{aligned}\Delta\mu_{\text{eff}}(\vec{x}) &= \mu_{\text{eff}}^P(\vec{x}) - \mu_{\text{eff}}^0(\vec{x}) &(6)\\ &= \alpha_c(\rho_c^P(\vec{x}) - \rho_c^0(\vec{x})) + \alpha_w(\rho_w^P(\vec{x}) - \rho_w^0(\vec{x})) &(7)\\ &= \alpha_c\Delta\rho_c(\vec{x}) + \alpha_w\Delta\rho_w(\vec{x}), &(8)\end{aligned}$$

where $\Delta\rho_w(\vec{x})$ is the change of the partial density of water between the reference and the wet states (local change of water content of a composite material point located originally at $\vec{x}$). Solving for $\Delta\rho_w(\vec{x})$ gives

$$\Delta\rho_w(\vec{x}) = \frac{\Delta\mu_{\text{eff}}(\vec{x}) - \alpha_c\Delta\rho_c(\vec{x})}{\alpha_w}. \tag{9}$$

Finally, assuming that the amount of residual water present in the dry state can be neglected, the partial densities of composite material and water in the wet state are given (again, in the dry state reference frame) by

$$\begin{aligned}\rho_c(\vec{x}) &= \rho_c^0(\vec{x}) + \Delta\rho_c(\vec{x}) = \frac{\mu_{\text{eff}}^0(\vec{x})}{\alpha_c} + \Delta\rho_c &(10)\\ \rho_w(\vec{x}) &= \Delta\rho_w(\vec{x}). &(11)\end{aligned}$$

3. Test case – polylactic acid/birch pulp composite material

The method discussed above was tested with polylactic acid/birch pulp composite material. The polylactic acid was Natureworks Ingeo 3001D polymer with MFI 22 and the birch pulp was provided by Metsä Fibre. The fibres and the matrix were compounded with a twin screw compounder and injection moulded to a dog bone shaped tensile test specimen containing 40 % fibre by mass. A cylindrical sample of 1.9 mm diameter was cut from the central part of the tensile test specimen using a high-precision milling machine. Care was taken not to damage the intact surface of the sample through which the water infiltration was to take place. The sample was glued on the top of a sample holder made of 1.9 mm diameter carbon fibre rod (see figure 1).

To construct a water chamber, the sample was placed and sealed in a long thin-walled polyethylene terephthalate (PET) tube with wall thickness ∼6.35 µm and inner diameter 1.98 mm (Vention Medical, United States). The gap between the sample and the tube inner wall was filled with cyanoacrylate glue that was drawn into the gap by capillary action. The

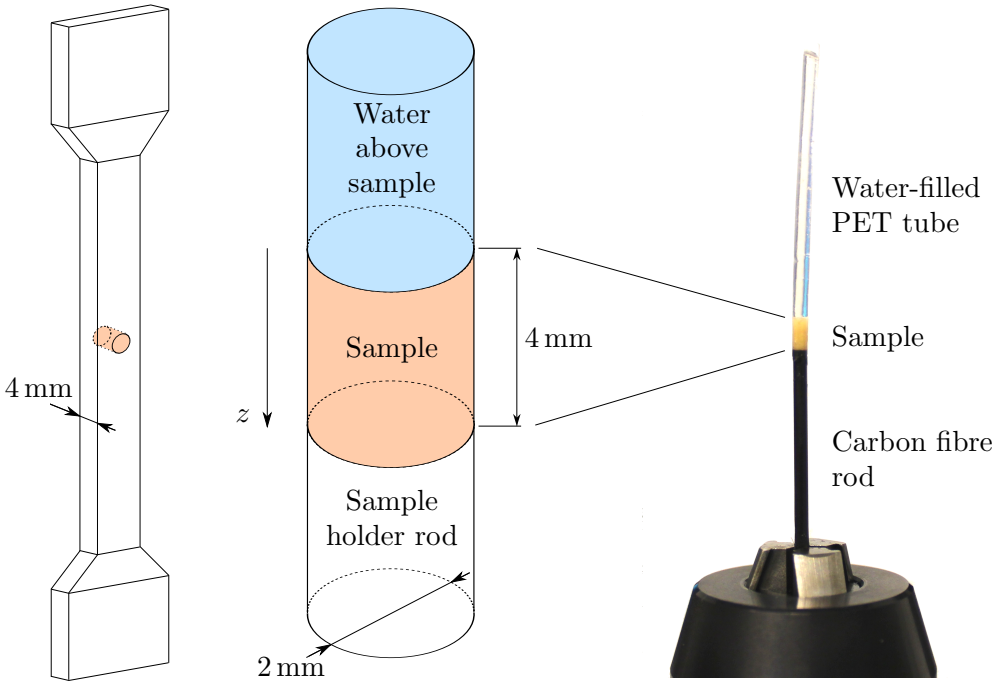

Figure 1. Schematic representation of sample location and orientation with respect to a tensile test specimen (left). The shaded part is the sample. The structure of the sample assembly (middle). Photograph of the realization of the sample assembly (right). The various diagrams are not drawn to scale.

diameter of the final sample, including the PET tube, is approximately 2 mm and its height is approximately 4 mm. The geometry and materials of the sample assembly, shown in figure 1, were selected to allow one-dimensional axial infiltration of water and as free swelling of the sample as possible during the wetting phase of the experiment.

After oven drying in 50°C for 24 h, the sample was imaged using Xradia microCT-400 device with 4.74 µm pixel size, 30 kV acceleration voltage and 3 W electron beam power. Total of 1129 projection images were acquired with 5 s exposure time, totalling in 3.5 h scan time. With the given settings the field-of-view of the tomographic image spans a cylinder of 2.2 mm diameter and height. The entire sample assembly can thus be kept within the field-of-view of the scanner in the radial direction, which is one of the basic requirements for faithful reconstruction of the sample. In the axial direction (z-direction in figure 1) three overlapping sub-scan tomograms had to be acquired to fit the whole 4 mm long sample into the combined field-of-view of the three images. For calibration purposes (see below) the combined image area was selected such that a part of the sample holder rod and a part of the water chamber were visible below and above the sample, respectively. The procedure thus yielded the dry state image $\mu^0_{\mathrm{eff}}(\vec{x})$ for each sub-scan region, see figure 2.

Wetting of the sample was initiated by adding water into the water chamber using a syringe and a needle mounted on a special stage that ensured controlled injection. Immediately after that, acquisition of the three sub-scan images sequentially with predetermined intervals was commenced. The intervals varied from 12 h in the beginning to one week at the end of the wetting process. The total duration of the process was 135 days.

After reconstruction and beam-hardening correction done using the standard utility software of the tomographic scanner, the images were found to contain relatively weak ring artefacts that are typically caused by spatial variation of the X-ray detector properties over its sensitive area.

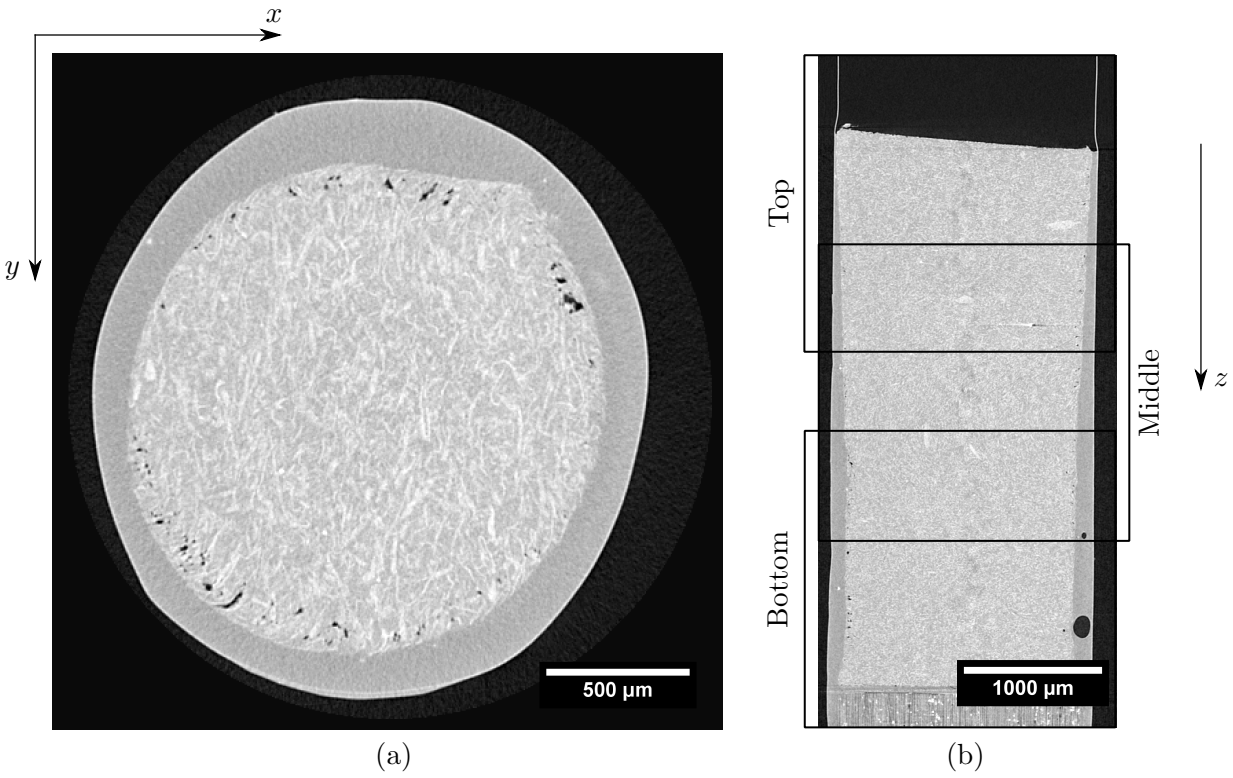

Figure 2. (a) A single horizontal slice of a tomographic image of the dry sample. The thin bright region on the edge of the sample is the PET tube, thick gray part is cyanoacrylate glue, bright small regions are parts of wood fibres and black holes near the edge of the sample are pores caused by milling. (b) A vertical slice of the dry sample showing the three overlapping sub-scan regions. The combined image includes a part of the carbon fibre sample holder rod visible in the bottom of the image and the lower part of the (empty) water chamber.

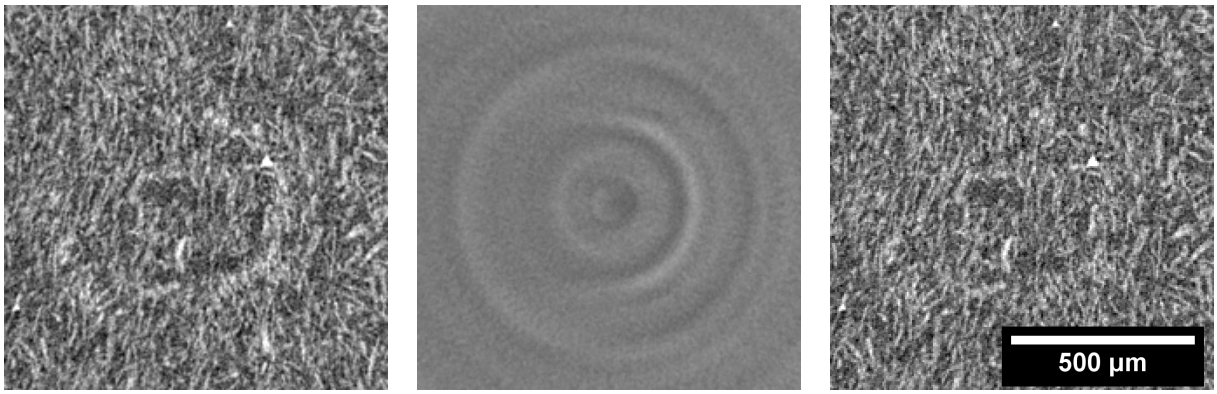

Figure 3. Removal of ring artefacts: A horizontal slice of an original image with notable ring artefact (left), of the normalization image produced as an average of 20 images of a homogeneous phantom sample (middle) and of a final corrected image (right). The scale bar applies to all the three images.

In order to alleviate the effect of ring artefacts in the final results, a phantom sample was made of highly homogeneous poly(methyl methacrylate) rod of diameter 2 mm, and imaged 20 times using the same settings as for the composite sample. The average image of these 20 images, containing virtually but the ring artefacts, was then used to normalize the original tomographic images thereby removing most of the ring artefacts (see figure 3).

We denote the sequence of final corrected images for a selected sub-scan region by $\mu_{\text{eff}}(j, \vec{x})$, where $j = 1, \ldots, N$ is the scan index such that $\mu_{\text{eff}}(1, \vec{x})$ is the image taken immediately after water injection at time $t = 0$ and $\mu_{\text{eff}}(N, \vec{x})$ is the image of the sample in its final state at time $t = 135$ days. The displacement fields $\vec{u}(j, \vec{x})$ between the dry state image $\mu^0_{\text{eff}}(\vec{x})$ and the wet state images $\mu_{\text{eff}}(j, \vec{x})$ were then found using equation (1). All the images were transformed into the reference frame of the corresponding dry state using equation (2) thus yielding images $\mu^P_{\text{eff}}(j, \vec{x})$. Spatial averages of $u_3(j, \vec{x})$ and $\mu^P_{\text{eff}}(j, \vec{x})$ over horizontal (x-y) sections of the sample were calculated for each value of the distance from the upper surface of the sample z, yielding the vertical profile of vertical displacement $u_3(j, z)$, and of attenuation coefficient $\mu^P_{\text{eff}}(j, z)$, respectively. The results from each sub-scan section were then patched together using linearly weighted interpolation within the sub-scan overlap regions, thereby forming the corresponding vertical profiles over the entire sample height.

The calibration constant α_w was obtained by

$$\alpha_w = \frac{\langle \mu_{\text{eff}}(1, z) \rangle_w}{\tilde{\rho}_w}, \tag{12}$$

where $\langle \cdot \rangle_w$ denotes average over part of the data corresponding to the region above the sample, containing solely water. The density of water was taken to be $\tilde{\rho}_w = 1000\,\text{kg/m}^3$. Similarly, the calibration constant α_c was obtained by

$$\alpha_c = \frac{\langle \mu^0_{\text{eff}}(z) \rangle_c}{\tilde{\rho}_c}, \tag{13}$$

where $\langle \cdot \rangle_c$ denotes average over the volume of the dry state sample. The density of the dry composite material was measured using a straightforward gravimetric method resulting in $\tilde{\rho}_c = (1280 \pm 20)\,\text{kg/m}^3$. The initial partial density of the composite material was set to

$$\rho^0_c(z) = \frac{\mu^0_{\text{eff}}(z)}{\langle \mu^0_{\text{eff}}(z) \rangle_c} \tilde{\rho}_c. \tag{14}$$

Finally, the partial densities of composite material and water for each j were calculated by substituting $u_3(j, z)$, $\mu^0_{\text{eff}}(z)$, $\mu^P_{\text{eff}}(j, z)$, α_c, α_w and $\rho^0_c(z)$ into Equations 3 – 11. As the final result, the measured evolution of water content in the sample is shown in figure 4.

4. Discussion and conclusions

A method for non-destructive quantitative measurement of time-dependent water content profile inside a composite material sample set in contact with water was introduced and applied to polylactic acid/birch pulp composite. The experimental set-up was designed to allow one-dimensional axial infiltration of water in a cylindrical composite material sample. As a result, measured water content profiles inside the sample were obtained at various times of wetting.

The method requires careful calibration and correction of various artefacts and sources of error inherent in X-ray tomographic techniques. In general, the measured water content profiles obtained in this preliminary study, shown in figure 4, appear qualitatively plausible and resemble those expected for a diffusive transport process, although not necessarily of simple linear form. In some of the measured profiles, anomalous structures appear indicating local deviation from

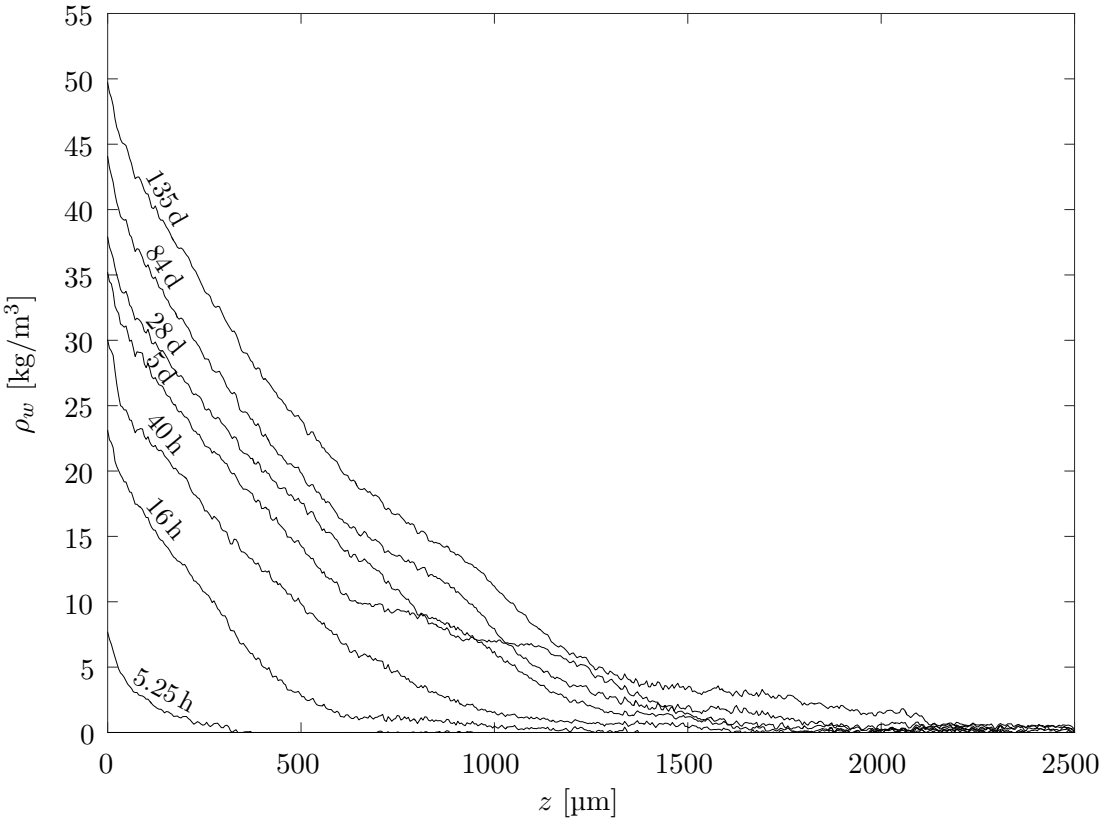

Figure 4. Measured water content profiles in the wood-fibre reinforced composite material sample for various values of wetting time, obtained using X-ray tomographic techniques. The origin of position z is at the surface of the sample exposed to water. For clarity, only a subset of all the measured profiles are shown.

the overall behaviour (see figure 4, near $z = 1000\,\mu\text{m}$). Without further investigation, it is not clear whether these anomalies are due to an error, or whether they arise for a physical reason such as presence of inhomogeneities in the sample.

In this first test of the method, a very small sample was used. This prevented valid independent verification of the results by gravimetric measurements, as done in, *e.g.*, [10]. However, based on the measured integrated water content, the total amount of water absorbed by the sample was somewhat less than expected based on independent gravimetric measurements done using larger samples. This might be due to water diffusing and evaporating through the mantle of the cylindrical sample, in spite of the thin layer of sealing glue and plastic tube. In future experiments larger samples and improved outer surface sealing should be used to facilitate quantitative validation of the method.

The detailed results obtained by the present method are useful in validating absorption models (see, *e.g.*, [12, 13]) and in quantifying the necessary material parameters related to water transport and hydromechanical behaviour of the composites. Although the method was applied here in virtually one-dimensional wetting geometry it can, in principle, be used to measure water content maps in a general three-dimensional case. Such extension of the method is left for future work.

References

[1] Campilho R 2016 *Natural Fiber Composites* (CRC Press)
[2] Joffre T, Wernersson E, Miettinen A, Luengo Hendriks C L and Gamstedt E K 2013 *Composites Science and Technology* **74** 52 – 59
[3] Cai Z 2008 *Forest products journal* **58** 41 – 45
[4] Leonard A, Blacher S, Marchot P, Pirard J P and Crine M 2005 *Canadian journal of chemical engineering* **83**(1) 127 – 131
[5] Ruiz de Argandoña V G, Rodriguez-Rey A, Celorio C, Calleja L and Suárez del Rio L M 2003 *Geological Society Special Publications* **215** 127–134
[6] Weder M, Brühwiler P A and Laib A 2006 *Textile Research Journal* **76** 18–26
[7] Lindsay J T, Matsubayashi M and Islam M N 1994 *Nuclear Instruments and Methods in Physics Research* A **353** 149 – 151
[8] Metwalli E, Hermes H E, Calzada E, Kulozik U, Egelhaaf S U and Muller-Buschbaum P 2016 *Physical Chemistry Chemical Physics* **18**(9) 6458 – 6464
[9] MacMillan M B, Schneider M H, Sharp A R and Balcom B J 2002 *Wood and fiber science* **34** 276 – 286
[10] Harjupatana T, Alaraudanjoki J and Kataja M 2015 *Applied Clay Science* **114** 386 – 394
[11] Stock S R 2009 *Microcomputed tomography* (CRC Press)
[12] Frandsen H L Selected constitutive models for simulating the hygromechanical response of wood
[13] Adhikary K B, Pang S and Staiger M P 2008 *Chemical Engineering Journal* **142** 190 – 198